

# Oxidative Stress Induces Disruption of the Axon Initial Segment

ASN Neuro  
November-December 2017: 1–13  
© The Author(s) 2017  
Reprints and permissions:  
sagepub.co.uk/journalsPermissions.nav  
DOI: 10.1177/1759091417745426  
journals.sagepub.com/home/asn



Kareem Clark<sup>1,2</sup>, Brooke A. Sword<sup>3</sup>, and Jeffrey L. Dupree<sup>1,3</sup>

## Abstract

The axon initial segment (AIS), the domain responsible for action potential initiation and maintenance of neuronal polarity, is targeted for disruption in a variety of central nervous system pathological insults. Previous work in our laboratory implicates oxidative stress as a potential mediator of structural AIS alterations in two separate mouse models of central nervous system inflammation, as these effects were attenuated following reactive oxygen species scavenging and NADPH oxidase-2 ablation. While these studies suggest a role for oxidative stress in modulation of the AIS, the direct effects of reactive oxygen and nitrogen species (ROS/RNS) on the stability of this domain remain unclear. Here, we demonstrate that oxidative stress, as induced through treatment with 3-morpholinopyridone (SIN-1), a spontaneous ROS/RNS generator, drives a reversible loss of AIS protein clustering in primary cortical neurons *in vitro*. Pharmacological inhibition of both voltage-dependent and intracellular calcium ( $\text{Ca}^{2+}$ ) channels suggests that this mechanism of AIS disruption involves  $\text{Ca}^{2+}$  entry specifically through L-type voltage-dependent  $\text{Ca}^{2+}$  channels and its release from  $\text{IP}_3$ -gated intracellular stores. Furthermore, ROS/RNS-induced AIS disruption is dependent upon activation of calpain, a  $\text{Ca}^{2+}$ -activated protease previously shown to drive AIS modulation. Overall, we demonstrate for the first time that oxidative stress, as induced through exogenously applied ROS/RNS, is capable of driving structural alterations in the AIS complex.

## Keywords

axon initial segment, calcium, calpain, oxidative stress, reactive nitrogen species, reactive oxygen species

Received July 3, 2017; Received revised September 28, 2017; Accepted for publication October 19, 2017

## Introduction

The axon initial segment (AIS) is a specialized region of the axon located at the junction between the somatodendritic and distal axonal domains that is essential for both action potential generation and the maintenance of neuronal polarity (Hedstrom et al., 2008; Buffington and Rasband, 2011). This complex consists of cytoskeletal scaffolding proteins ankyrin-G (AnkG) and  $\beta$ IV-spectrin, which cluster the high density of voltage-gated ion channels required for action potential initiation and modulation (Jenkins and Bennett, 2001). The AIS is a highly dynamic and plastic structure regulated by changes in neuronal activity (Yamada and Kuba, 2016), but its integrity is compromised consequentially of a variety of pathological central nervous system (CNS) insults. These include models of epilepsy (Wimmer et al., 2010; Harty et al., 2013), ischemic injury (Schafer et al., 2009; Hinman et al., 2013), traumatic brain injury (Baalman

et al., 2013; Greer et al., 2013; Vascak et al., 2017), Alzheimer's disease (Leon-Espinosa et al., 2012; Sun et al., 2014; Marin et al., 2016; Zempel et al., 2017), and multiple sclerosis (MS) (Hamada and Kole, 2015; Clark et al., 2016). While the AIS is frequently and extensively targeted for disruption in CNS pathology, the

<sup>1</sup>Department of Anatomy and Neurobiology, Virginia Commonwealth University, Richmond, VA, USA

<sup>2</sup>Neuroscience Curriculum, Virginia Commonwealth University, Richmond, VA, USA

<sup>3</sup>Hunter Holmes McGuire VA Medical Center, Richmond, VA, USA

### Corresponding Author:

Jeffrey L. Dupree, Department of Anatomy and Neurobiology, PO Box 980709, 1101 East Marshall Street, Sanger Hall Room 9048, Virginia Commonwealth University, Richmond, VA 23298, USA.  
Email: jeffrey.dupree@vcuhealth.org



mechanisms underlying altered stability of this domain have not been fully elucidated.

Our laboratory has previously demonstrated that AIS integrity is targeted for disruption in inflammatory environments. For example, induction of experimental autoimmune encephalomyelitis, a model commonly used to mimic the inflammatory component of MS (Kipp et al., 2017), resulted in severe disruption of the AIS domain, which was preceded by and correlated with microglial reactivity and increased contact (Clark et al., 2016). Similarly, peripheral injection of lipopolysaccharide (LPS), a classic model of systemic inflammation, was sufficient to drive the loss of AIS protein clustering, which was reversed following resolution of the inflammatory response (Benusa et al., 2017). In both of these inflammatory models, treatment with Didox, a novel scavenger of reactive oxygen and nitrogen species (ROS/RNS) (Mayhew et al., 2002; Turchan et al., 2003; Matsebatlela et al., 2015), prevented and reversed the AIS pathology (Clark et al., 2016; Benusa et al., 2017). In addition, LPS injection in mice deficient in the major ROS producing enzyme NADPH oxidase 2 (Pollock et al., 1995) resulted in the complete preservation of the AIS (Benusa et al., 2017). Together, these data highlight a potential role for ROS and RNS in the alteration of AIS protein clustering; however, direct evidence that ROS/RNS are capable of driving AIS disruption is lacking. Here, to address this void in our understanding, we investigate the effect of exogenously applied ROS/RNS on AIS stability in primary cortical neurons *in vitro*, utilizing the spontaneous ROS/RNS generator SIN-1 (Singh et al., 1999).

Our findings demonstrate that oxidative stress, induced through exogenous application of ROS/RNS, is sufficient to drive structural disruption of the AIS protein complex. Pharmacological inhibition of voltage-dependent calcium channels (VDCCs), intracellular calcium ( $\text{Ca}^{2+}$ ) stores, and enzymatic activity suggests this mechanism of ROS/RNS-induced AIS disruption to involve cytosolic  $\text{Ca}^{2+}$  entry extracellularly through L-type VDCCs, and intracellularly from  $\text{IP}_3$ -gated store release, as well as calpain protease activation.

## Materials and Methods

### Animals

Timed pregnant embryonic Day 14 (E14) c57bl/6 mice were purchased from Charles River (Wilmington, MA) and maintained in the Virginia Commonwealth University Division of Animal Resources (VCU DAR) or the McGuire Veterans Affairs Medical Center (VAMC) vivariums, respectively, which are both AAALAC accredited facilities. Timed pregnant mice were maintained in the facilities until pups were removed

on embryonic Day 15. Animals were maintained on an alternating 12-hr light and dark cycle and food and water were provided ad libitum. All procedures were conducted in accordance with the methods outlined in approved VCU and McGuire VAMC IACUC protocols.

### Primary Neuronal Cultures

Primary cortical neuron cultures were prepared from cerebral cortices of E15 mouse pups. Timed pregnant females were anesthetized with isoflurane and sacrificed by decapitation. Pups were removed and decapitated to allow for removal of the brains. Following removal of the meninges, cortices were incubated on ice in Accutase<sup>®</sup> Cell Detachment Solution (Innovative Cell Technologies, San Diego, CA) and dissociated step-wise using 1,000- $\mu\text{L}$  and 200- $\mu\text{L}$  sized pipette tips. Cells were counted and diluted in plating medium consisting of Neurobasal<sup>®</sup> medium (Thermo Fisher Scientific, Waltham, MA; Formulation detailed in Supplementary Table 1) supplemented with glutamate (25  $\mu\text{M}$ , Sigma-Aldrich, St. Louis, MO), glutamine (0.5 mM, Thermo Fisher Scientific, Waltham, MA), Antibiotic-Antimycotic (Thermo Fisher Scientific, Waltham, MA), and B-27<sup>®</sup> supplement (Thermo Fisher Scientific, Waltham, MA). Cells were then plated at a density of 3000 cells/ $\text{cm}^2$  on poly-d-lysine (1 mg/mL; Sigma-Aldrich, St. Louis, MO)-coated glass coverslips (12 mm) in 24-well plates. Following cell attachment, wells were filled with the medium described above, in which the B-27<sup>®</sup> supplement was replaced with B-27<sup>®</sup> supplement minus antioxidants (Thermo Fisher Scientific, Waltham, MA). All experiments were performed starting at 12 days *in vitro* (DIV).

### SIN-1 and Pharmacological Treatments

Twelve DIV neurons were treated with SIN-1 (3-Morpholinopyridone hydrochloride, Sigma-Aldrich, St. Louis, MO) diluted in the maintenance media described above at concentrations ranging from 0.1 to 100  $\mu\text{M}$  and analyzed at 3, 6, 12, 24, or 72 hr post-treatment. All pharmacological reagents were added simultaneously with SIN-1 and included ethylene glycol-bis( $\beta$ -aminoethyl ether)-N,N,N',N'-tetraacetic acid (EGTA) (0.001 to 2 mM),  $\text{NiCl}_2$  (0.1 to 50  $\mu\text{M}$ ), (S)-(-)-Bay K8644 (0.00001 to 50  $\mu\text{M}$ ), MK-801 (0.001 to 50  $\mu\text{M}$ ), 2-APB (0.1 to 50  $\mu\text{M}$ ), and FK-506 (0.001 to 50  $\mu\text{M}$ ) obtained from Sigma-Aldrich (St. Louis, MO), as well as  $\omega$ -Conotoxin MVIIC (0.001 to 50  $\mu\text{M}$ ), nifedipine (0.001 to 50  $\mu\text{M}$ ), ryanodine (0.001 to 50  $\mu\text{M}$ ), and MDL 28170 (0.001 to 50  $\mu\text{M}$ ) obtained from Tocris Bioscience (Avonmouth, Bristol, England). Stock dilutions of all pharmacological reagents were prepared in DMSO (Thermo Fisher Scientific, Waltham, MA) with

subsequent dilutions performed in culture medium, except for EGTA, NiCl<sub>2</sub>, and  $\omega$ -Conotoxin MVIIC, in which all dilutions were performed in culture medium. While a larger concentration range of pharmacological inhibitors and activators was tested, only noncytotoxic concentrations were included in the presented data. All SIN-1 and pharmacological treatments were performed in three separate cell culture preparations ( $n=3$ ). Within each preparation, three technical replicates at the 24-hr time point were performed.

### Measurement of Calpain Activity

Calpain activity was quantified using a fluorometric assay kit (Biovision, Milpitas, CA) according to the manufacturer's instructions. Briefly, neurons were treated with the extraction buffer provided by the manufacturer to extract cytosolic proteins while preventing the autoactivation of calpain during the extraction procedure. The neuronal supernatant was then incubated with a calpain substrate (Ac-LLY-AFC) which fluoresces at 505 nm upon cleavage. Fluorescence intensities at each SIN-1 concentration were measured on a spectrophotometric microplate reader and compared against an untreated sample at each time point. Six coverslips of neurons were pooled at each time point and SIN-1 concentration. Data from these measurements are presented as relative fluorescence units as a percent increase over untreated samples. A total of three separate culture preparations ( $n=3$ ), each run in three technical replicates, were compared at each measurement. Statistical comparisons were made by repeated measures one-way analysis of variance (ANOVA) with a Dunnett's multiple comparisons post hoc test. All graphing and statistical analyses were performed using GraphPad Prism version 6.03 for Windows (GraphPad Software, San Diego, CA).

### Immunofluorescence

Cells were immunolabeled with the appropriate primary and secondary antibodies (see below) as described previously (Shepherd et al., 2012; Clark et al., 2016; Benusa et al., 2017), with the modification that cells were fixed with 4% paraformaldehyde (Ted Pella, Redding, CA) for 5 min and permeabilized with ice cold methanol (Fisher Scientific, Waltham, MA). Slides were mounted with Vectashield<sup>TM</sup> mounting medium with DAPI (Vector Laboratories, Burlingame, CA) and imaged using confocal microscopy.

### Antibodies

Axon initial segments were visualized using mouse monoclonal antibodies directed against AnkG (NeuroMab, Davis, CA; N106/36, 1:200) or  $\beta$ IV spectrin (a generous gift from Dr. Matthew Rasband, Baylor College of

Medicine; 1:500). Neurons were identified using either NeuN (Millipore; Billerica, MA; 1:1000) or MAP2 (Sigma-Aldrich, St. Louis, MO; 1:500) antibodies. All secondary antibodies for immunofluorescence were purchased from Invitrogen Life Technologies (Grand Island, NY; Alexa<sup>TM</sup> Fluor) and used at a dilution of 1:500.

### Confocal Microscopy or Quantitation

**Image collection.** All images were collected using a Zeiss LSM 710 confocal laser scanning microscope (Carl Zeiss Microscopy, LLC, Thornwood, NY) housed in the VCU Department of Anatomy and Neurobiology Microscopy Facility. Confocal z-stacks, each spanning an optical distance of 10  $\mu$ m, using a pin hole of 1 Airy disc unit and Nyquist sampling were collected from three technical replicate coverslips (12 mm) per treatment and time point resulting in 12 images per experimental group for AIS quantitation (~ 600 neurons per treatment group). All comparisons were made using three independent culture preparations ( $n=3$ ). Images were taken with a 20 $\times$  objective with a numerical aperture of 1.4; optical slice thickness was 0.49  $\mu$ m, using a scan average of 2. X, Y, and Z image dimensions were 212.43  $\mu$ m  $\times$  212.43  $\mu$ m  $\times$  10.00  $\mu$ m, respectively. The gain and offset values were kept constant for all images.

**AIS quantitation.** AIS stability was determined using ImageJ analysis software by manually counting initial segments from maximum intensity projection images resulting in the analysis of >600 AISs per experimental treatment and time point. The number of neurons in a field of view (FOV) was also determined in the same images used for AIS analysis by counting NeuN-positive cells. Data are presented as the percent of NeuN-positive cells with an associated AIS as a percent of the control. One-way ANOVAs with Tukey's Honest Significant Difference post hoc tests were performed for these comparisons. All graphing and statistical analyses were performed using GraphPad Prism version 6.03 for Windows (GraphPad Software, San Diego, CA).

**Cell viability quantitation.** The extent of neuronal survival following SIN-1 treatment was determined using a propidium iodide (PI) exclusion assay. Prior to paraformaldehyde fixation, cells were treated with a 0.01-mg/mL PI (Molecular Probes, Eugene, OR) solution for 10 min. Cells were then fixed and immunolabeled for NeuN as described above. The number of PI-positive and NeuN-positive cells was manually counted from maximum intensity projection images using ImageJ analysis software. Data are presented as the percent of NeuN-positive cells negative for PI as a percent of the control (% neuronal survival). One-way ANOVAs with Tukey's Honest Significant Difference post hoc tests were performed for these comparisons. All graphing and statistical analyses were performed using GraphPad

Prism version 6.03 for Windows (GraphPad Software, San Diego, CA).

**Measurement of ROS production.** Quantification of neuronal ROS production induced by SIN-1 treatment was performed using the CellROX<sup>®</sup> Green Reagent kit (Thermo Fisher Scientific, Waltham, MA) according to the manufacturer's instructions. Briefly, 12 DIV primary cortical neurons grown on coverslips were treated with SIN-1 at concentrations ranging from 0.1 to 100  $\mu$ M and analyzed 3, 6, 12, 24, or 72 hr posttreatment. Cells were incubated for 30 min at 37°C with CellROX<sup>®</sup> reagent at a concentration of 5  $\mu$ M. Coverslips were rinsed with PBS and mounted on slides with Vectashield<sup>™</sup> hard-set mounting medium with DAPI (Vector Laboratories, Burlingame, CA), and imaged using confocal microscopy as described above. The CellROX<sup>®</sup> green fluorescence intensity was measured from maximum intensity projection images using ImageJ analysis software. Data from these measurements are presented as the percent fluorescence increase over the untreated at each SIN-1 treatment concentration and time point. Data from these measurements are presented as relative fluorescence units as a percent increase over untreated samples. A total of three separate culture preparations ( $n=3$ ) were compared at each measurement. Statistical comparisons were made by repeated measures one-way ANOVA with a Dunnett's multiple comparisons post hoc test. All graphing and statistical analyses were performed using GraphPad Prism version 6.03 for Windows (GraphPad Software, San Diego, CA).

## Results

### ROS/RNS Generator, SIN-1, Induces Primary Neuronal Oxidative Stress In Vitro

To directly test the effect of ROS/RNS on AIS stability, we treated primary cortical neurons *in vitro* with the NO and superoxide donor SIN-1 (Singh et al., 1999; Trackey et al., 2001; Rocchitta et al., 2005; Zhaowei et al., 2014). Optimal SIN-1 treatment conditions were first determined using a combination of cell death analysis and a ROS production assay to identify SIN-1 concentrations that generated ROS/RNS without inducing cortical neuron death. Our first step was to administer the SIN-1 reagent, ranging in concentrations from 0.1  $\mu$ M to 100  $\mu$ M consistent with previous studies (Trackey et al., 2001; Rocchitta et al., 2005; Zhaowei et al., 2014), to determine the maximum SIN-1 concentration that could be tolerated by the cultured cells. Neuronal survival was assessed by the PI exclusion assay 24 hr posttreatment, a time point consistent with previous SIN-1 cytotoxicity studies (Trackey et al., 2001). As shown in Figure 1(a) to (f) and (m), significant cell death was observed at the highest concentrations (50  $\mu$ M and 100  $\mu$ M), while no cell loss occurred at the concentrations of 25  $\mu$ M and below.

Specifically, the percent of NeuN positive cells that were also PI negative (defined as % neuronal survival) 24 hr after the addition of SIN-1 was  $90.7\% \pm 6.6\%$ ,  $84.0\% \pm 5.9\%$ ,  $91.6\% \pm 4.9\%$ , and  $89.0\% \pm 9.5\%$  for SIN-1 concentrations of 0.1, 1, 10, and 25  $\mu$ M, respectively. Significant neuronal loss, however, was detected at SIN-1 concentrations of both 50  $\mu$ M ( $54.4\% \pm 12.5\%$ ,  $p = .0004$ ; Figure 1(m)) and 100  $\mu$ M ( $4.1\% \pm 0.42\%$ ,  $p < .0001$ ; Figure 1(f) and (m)). Therefore, these findings indicated that 25  $\mu$ M was an appropriate concentration for SIN-1 treatment to ensure that cell death was not induced.

Our initial studies to identify optimal SIN-1 concentrations were conducted at the 24-hr time point based on previous work (Trackey et al., 2001). However, to better understand the profile of ROS/RNS production in our culture system, we employed the CellROX<sup>®</sup> Green assay, a fluorogenic cell-permeable probe which fluoresces upon oxidation by ROS (Liu et al., 2014; Isaev et al., 2016), to quantify levels of neuronal ROS over time. No significant increase in neuronal ROS levels was detected at 3 (Figure 1(h) and (n)) and 6 hr (Figure 1(i) and 9(n)) post SIN-1 treatment, at a concentration of 25  $\mu$ M (the highest noncytotoxic concentration), as compared with the untreated cultures (Figure 1(g) and (n)). However, by 12 hr (Figure 1(j) and (n)) post SIN-1 addition, ROS levels were significantly increased with the levels peaking by 24 hr (Figure 1(k) and (n)) post SIN-1 treatment. By 72 hr (Figure 1(l) and (n)) post SIN-1 addition, ROS production returned to baseline levels indicating a resolution of the oxidative insult. With an established time course of SIN-1-induced oxidative stress through the CellROX<sup>®</sup> assay, we next asked whether AIS integrity was compromised as a result of this insult.

### Exogenously Applied ROS/RNS Induce AIS Disruption In Vitro

To assess the effects of exogenously applied ROS/RNS on AIS stability, primary cortical neurons were treated with SIN-1 at all of the noncytotoxic concentrations tested above (0.1 to 25  $\mu$ M) and subsequently double immunolabeled for AnkG and NeuN at 3, 6, 12, and 24 hr posttreatment. Data are presented as the percent of neurons (defined as NeuN+ cells) with an associated AIS (defined as AnkG+). Representative images for only the 25  $\mu$ M SIN-1 treatments are shown for each time point (Figure 2(b) to (f)). No significant alteration in AIS integrity was observed at any of the tested SIN-1 concentrations at (0.1 to 25  $\mu$ M) 3 hr (Figure 2(b) and (g)), 6 hr (Figure 2(c) and (h)), or 12 hr (Figure 2(d) and (i)) posttreatment as compared with the nontreated cultures (Figure 2(a)). Similarly, at 24 hr (Figure 2(j)), neither 0.1  $\mu$ M nor 1  $\mu$ M of SIN-1 was sufficient to induce disruption of the AIS. However, AIS loss was

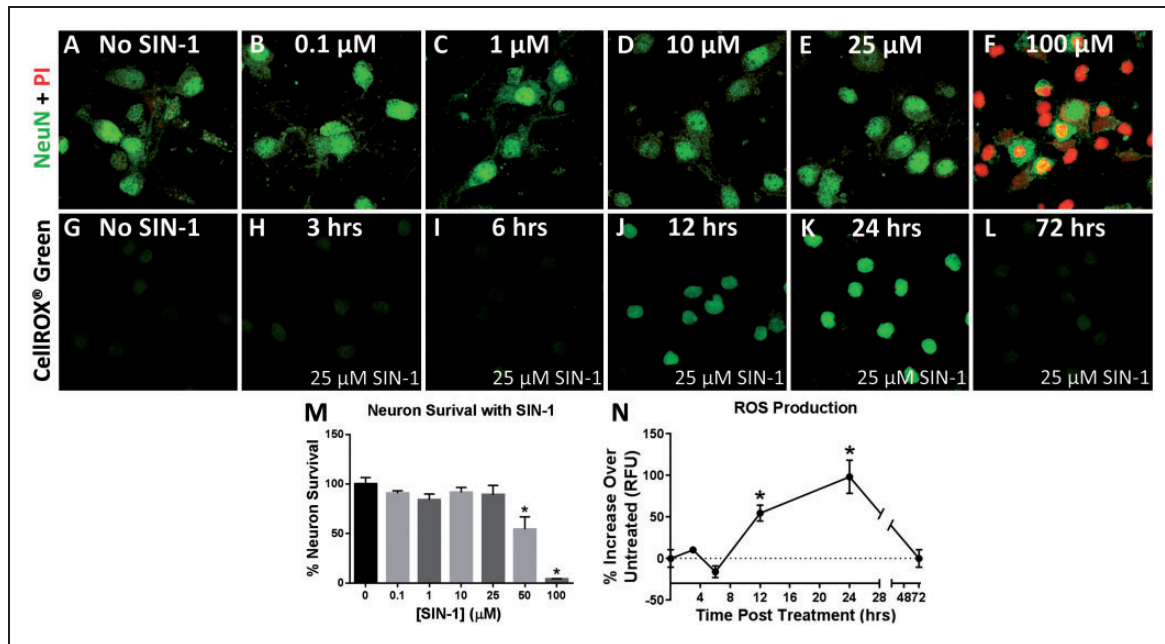


**Figure 1.** ROS/RNS generator, SIN-1, induces oxidative stress *in vitro*. Cortical neurons (NeuN+ cells, green) treated with ((b) to (f)) and without (a) SIN-1 at increasing concentrations reveal no propidium iodide (PI) staining at concentrations of 25  $\mu\text{M}$  and below ((b) to (e)) 24 hr posttreatment; however, robust staining was present at concentrations of 50  $\mu\text{M}$  (not shown) and 100  $\mu\text{M}$  (f). Quantitation of percent neuronal survival, determined as the percentage of NeuN+ cells that were also PI- (as a percent of the untreated cells), revealed significant cell death at SIN-1 concentrations of 50  $\mu\text{M}$  and 100  $\mu\text{M}$  (m). The CellROXR Green assay for detection of ROS production by the cortical neurons revealed baseline levels of ROS at  $\leq 6$  hr post SIN-1 treatment ((g) to (i), (n)) with significantly elevated levels at 12 hr ((j) and (n)), peak levels at 24 hr ((k) and (n)) and a return to baseline by 72 hr ((l) and (n)). Asterisks represent a significant difference from the SIN-1 untreated group (\* $p < .05$ ).

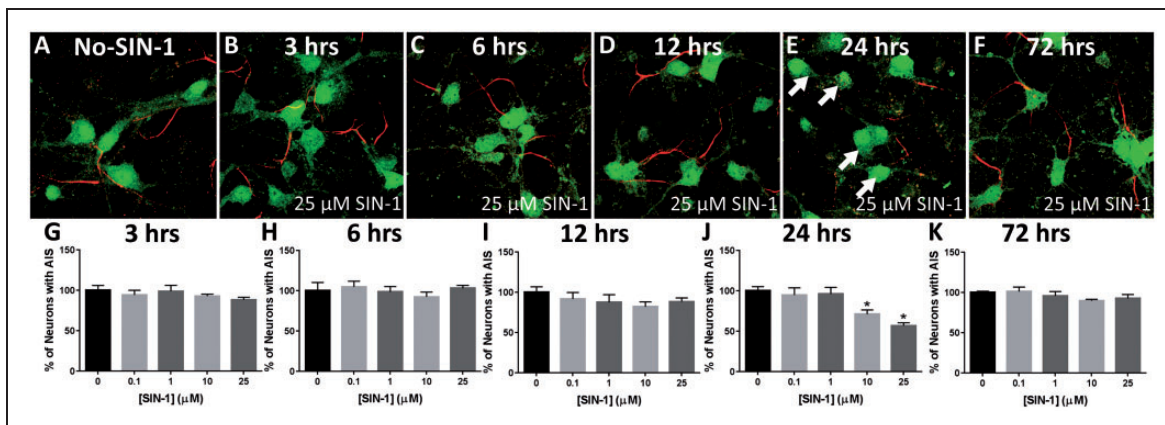


**Figure 2.** Exogenous ROS/RNS drive disruption of the AIS *in vitro*. Axon initial segments of cultured cortical neurons maintain their integrity with no SIN-1 treatment (a) or 3 ((b) and (g)), 6 ((c) and (h)), or 12 ((d) and (i)) hr following exposure to 25  $\mu\text{M}$  SIN-1, a concentration that did not induce cell death. However, at this same concentration, a significant dose-dependent reduction in the number of cortical neurons (NeuN+, green) that presented ankyrin-G (red) positive AISs was observed 24 hr after SIN-1 exposure (white arrows; (e) and (j)). By 72 hr post SIN-1 exposure, AIS integrity was restored ((f) and (k)) demonstrating the reversibility of AIS disruption and further indicating that AIS loss was not a consequence of cell death. Asterisks represent a significant difference from the SIN-1 untreated group (\* $p < .05$ ).

observed 24 hr after SIN-1 addition at concentrations of 10  $\mu\text{M}$  (Figure 2(j);  $p = .034$ ) and 25  $\mu\text{M}$  (Figure 2(e) and (j);  $p = .003$ ) with a significant reduction in the percent of neurons with an associated AIS of  $29.0\% \pm 5.2\%$  and

$43.2\% \pm 3.7\%$ , respectively. Results from AnkG quantitation were confirmed by immunolabeling for  $\beta\text{IV}$ -spectrin, another AIS protein crucial for domain stability (data not shown).

Since the CellROX<sup>®</sup> assay indicated a return to baseline levels of ROS/RNS by 72 hr, we next analyzed AIS integrity at this late time point to determine whether the ROS/RNS-induced AIS disruption is reversible. Interestingly, recovery was observed 72 hr following SIN-1 treatment at both the 10  $\mu$ M (Figure 2(k)) and 25  $\mu$ M (Figure 2(f) and (k)) concentrations. To ensure that the recovery in the percentage of AIS+ cells was not due to a loss of neurons that lacked positively labeled AISs, the relative number of NeuN+ cells was compared between the treated and nontreated groups. No significant difference was observed between groups (data not shown) indicating that NeuN+ cells that lost their AISs did not die, but recovered from the SIN-1 treatment and restored their AIS. This recovery at 72 hr posttreatment corresponds to a return to baseline of neuronal ROS levels as shown in Figure 1(l) and (n). Overall, these data provide a time course for ROS/RNS-induced AIS disruption in our *in vitro* system, allowing for subsequent pharmacological manipulations to elucidate the underlying mechanism. All further experiments were performed 24 hr following treatment of 25  $\mu$ M SIN-1, the time point of peak AIS loss, and the highest noncytotoxic concentration of SIN-1, respectively.

### ROS/RNS-Induced AIS Disruption Requires Extracellular Ca<sup>2+</sup>

Calcium (Ca<sup>2+</sup>) is central to most previously identified mechanisms of AIS modulation, during both activity-dependent plasticity (Yamada and Kuba, 2016) as well as pathological insult (Stoler and Fleidervish, 2016). To determine if ROS/RNS-induced AIS disruption involves extracellular Ca<sup>2+</sup> entry, neurons were pretreated with the nonmembrane permeable Ca<sup>2+</sup>-chelating agent EGTA, prior to SIN-1 addition. EGTA pretreatment at concentrations of 0.001 mM and 0.01 mM were not

sufficient to prevent the AIS disruption previously observed (Figure 3(d)), and SIN-1 treated cells exposed to these concentrations were indistinguishable from those without EGTA (Figure 3(b) and (d)). EGTA concentrations of 1 mM (Figure 3(d)) and 2 mM (Figure 3(c) and (d)), however, were capable of attenuating the AIS disruption, resulting in the preservation of 81.9%  $\pm$  0.8% ( $p = .0004$ ) and 94.9%  $\pm$  0.7% ( $p < .0001$ ) of neurons with an associated AIS, respectively, as compared with the 62.3%  $\pm$  1.6% observed with SIN-1 treatment alone. Similar to other previously established models of AIS plasticity and injury (Schafer et al., 2009; Stoler and Fleidervish, 2016; Yamada and Kuba, 2016), these data demonstrate that extracellular Ca<sup>2+</sup> is central to AIS disruption; however, we implicate ROS/RNS as upstream activators of this degenerative pathway.

### L-Type Voltage-Dependent Calcium Channels Are Required for ROS/RNS-Induced AIS Disruption

While the importance of extracellular Ca<sup>2+</sup> entry has been demonstrated with EGTA, the entry point for Ca<sup>2+</sup> into the cell during ROS/RNS-induced AIS modulation remains unclear. To address this, we pretreated neurons with a series of inhibitors to the known types of voltage-dependent calcium channels prior to SIN-1 treatment (Catterall, 2011). Inhibition of T- and R-type VDCCs by NiCl<sub>2</sub> (Bhattacharjee et al., 1997; Evans et al., 2013) revealed no significant attenuation of SIN-1-induced AIS disruption at the range of concentrations tested (0.1 to 50  $\mu$ M; Figure 4(c) and (g)). Similarly, no AIS protection was observed following application of the P-, Q-, and N-type VDCC inhibitor  $\omega$ -Conotoxin MVIIC (0.0001 to 1  $\mu$ M; Figure 4(d) and (h)). Concentrations of these inhibitors higher than those presented resulted in significant neuronal death (data not shown). In addition, specific inhibition of L-type VDCCs with nifedipine

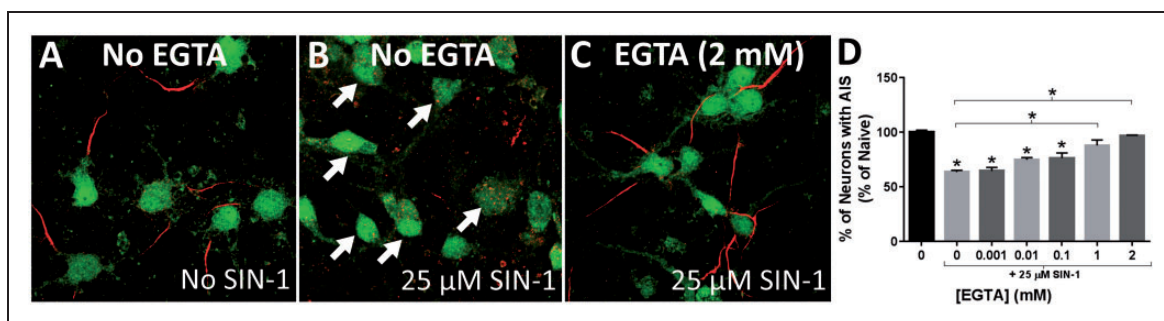


**Figure 3.** ROS/RNS-induced AIS disruption is attenuated following chelation of extracellular Ca<sup>2+</sup>. The loss of AIS labeling (white arrows) following exposure to 25  $\mu$ M SIN-1 (b) was inhibited by the addition of EGTA (c) to the medium prior to SIN-1 treatment. The extent of AIS maintenance was directly dependent on the dose of EGTA (d). An asterisk with an associated bracket indicates significant differences between treated groups; asterisks without an associated bracket represent a significant difference from the SIN-1 untreated group (a, \* $p < .05$ ). NeuN, green; AnkG, red.

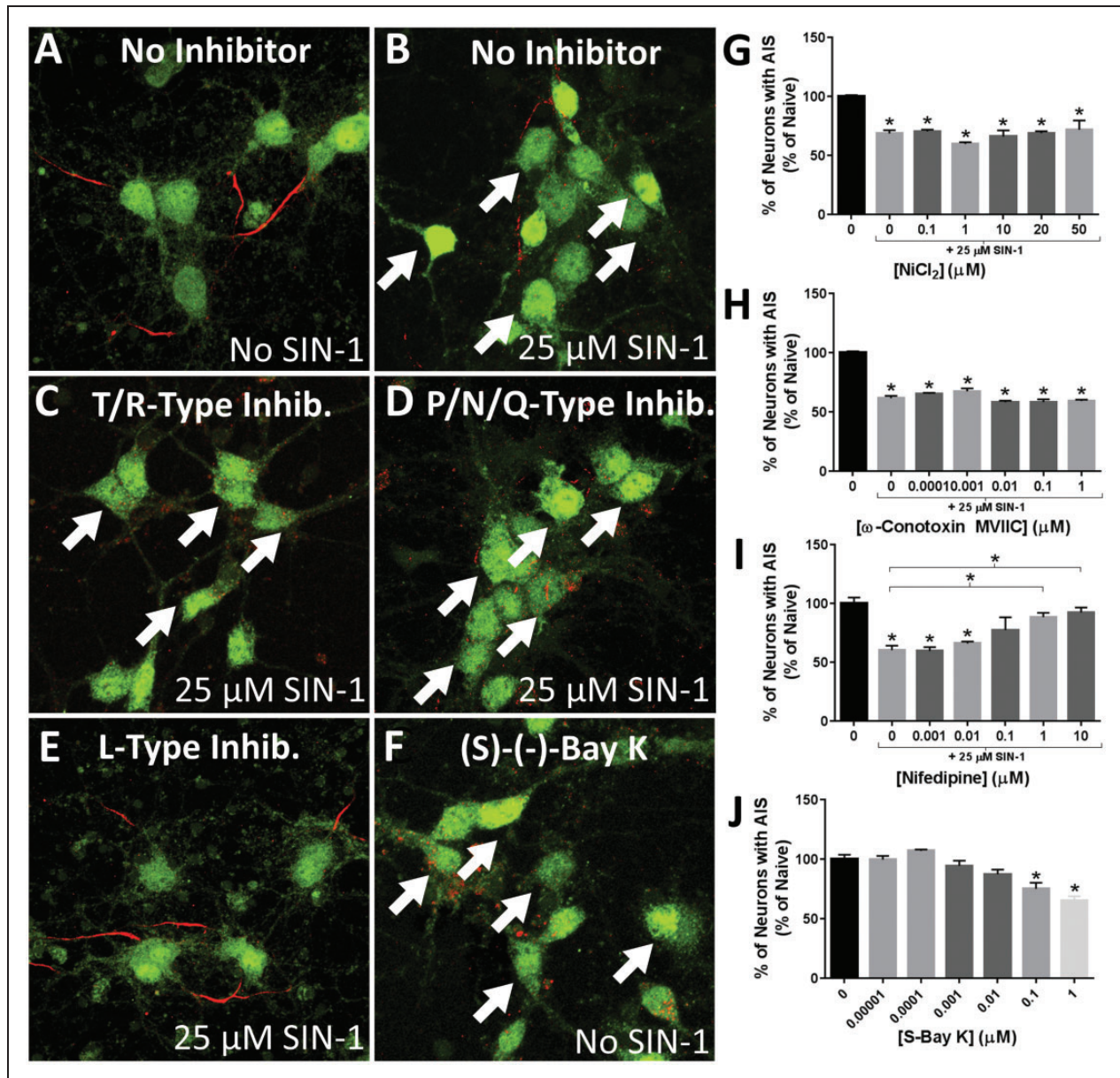


**Figure 4.** L-type voltage-dependent calcium channels are required for ROS/RNS-induced AIS disruption. Similar to SIN-1 treated neurons without inhibitor pretreatment (b), neurons (NeuN+, green) treated with inhibitors directed against T/R- ((c) and (g)) or P/N/Q-type ((d) and (h)) calcium channels prior to SIN-1 exposure presented with significant loss (white arrows) in AIS labeling (AnkG, red). In contrast, cultured cortical neurons treated with an L-type calcium channel inhibitor ((e) and (i)) resulted in a significant preservation of the AISs. Further demonstrating a role for L-type calcium channels in mediating AIS alterations, cortical neurons treated with (S)-(-)-Bay K 8644 also resulted in a significant disruption of the AISs ((f) and (j)). Asterisks without an associated bracket represent a significant difference from the SIN-1 untreated group (a, \* $p < .05$ ).

(Nguemo et al., 2013) at concentrations of 0.001 to 0.1  $\mu$ M was not sufficient to protect AIS integrity. However, attenuation of SIN-1-induced AIS disruption was observed following pretreatment with the L-type specific VDCC inhibitor at concentrations of 1  $\mu$ M and 10  $\mu$ M (Figure 4(e) and (i)) resulting in the preservation of 88.3%  $\pm$  3.66% ( $p = .0147$ ) and 92.1%  $\pm$  4.3% ( $p = .0055$ ) of AISs respectively, as compared with the

60.2%  $\pm$  3.9% percent observed with SIN-1 treatment alone.

We then asked whether Ca<sup>2+</sup> flow through L-type VDCCs in the absence of SIN-1 was sufficient to drive disruption of the AIS. To address this, a selective irreversible activator of L-type channels, (S)-(-)-Bay K 8644 (Ravens and Schöpper, 1990; Fusi et al., 2017), was used at concentrations ranging from 0.00001 to 1  $\mu$ M with AIS

assessment performed 24 hr posttreatment. This treatment resulted in a significant reduction in the percent of neurons with an associated AIS at concentrations of 0.1  $\mu\text{M}$  and 1  $\mu\text{M}$  by  $22.6\% \pm 3.9\%$  ( $p = .0002$ ) and  $32.5\% \pm 3.9\%$  ( $p < .0001$ ), respectively (Figure 4(f) and (j)). Importantly, these concentrations of (S)-(-)-Bay K 8644 did not result in neuronal death as determined by the PI exclusion assay described above (data not shown). Overall, these data suggest that ROS/RNS-mediated disruption of the AIS involves extracellular  $\text{Ca}^{2+}$  flow specifically through L-type VDCCs, and that activation of these channels, independently of SIN-1, is sufficient to drive similar AIS alterations.

### ROS/RNS-Mediated AIS Modulation Involves $\text{IP}_3$ -Gated $\text{Ca}^{2+}$ Stores

Because AIS stability is heavily dependent on the level of intracellular  $\text{Ca}^{2+}$  (Stoler and Fleidervish, 2016; Yamada and Kuba, 2016) and on the function of VDCCs for ROS/RNS-mediated AIS disruption, we next asked if release from intracellular stores is involved in this SIN-1-induced insult. Prior to SIN-1 addition, neurons were pretreated with inhibitors to both ryanodine and inositol 1,4,5-trisphosphate ( $\text{IP}_3$ ) receptors, the two major mediators of  $\text{Ca}^{2+}$  release from intracellular stores (Marks, 1997;

Evans et al., 2013). Inhibition of ryanodine receptors with ryanodine at concentrations of 0.001 to 10  $\mu\text{M}$  did not result in protection of the AIS from SIN-1-induced disruption (Figure 5(c) and (e)). Concentrations greater than 10  $\mu\text{M}$  resulted in significant neuronal death (data not shown). Conversely, pretreatment with  $\text{IP}_3$  receptor inhibitor 2-Aminoethoxydiphenyl borate (2-APB) was capable of significantly preserving AIS integrity in a dose-dependent manner at concentrations of 10  $\mu\text{M}$  and 20  $\mu\text{M}$ , resulting in the preservation of  $80.4\% \pm 7.3\%$  ( $p = .0290$ ) and  $95.1\% \pm 2.7\%$  ( $p = .0002$ ) of neurons with an intact AIS, respectively (Figure 5(d) and (f)). Interestingly, low concentrations of 2-APB ( $<10 \mu\text{M}$ ) result in the release of  $\text{Ca}^{2+}$  from  $\text{IP}_3$ -gated intracellular stores (DeHaven et al., 2008), a possible explanation for the exacerbated effect of SIN-1 on the AIS at the 0.1  $\mu\text{M}$  concentration (Figure 5(f);  $p = .0010$ ). Taken together, these data highlight an important role for  $\text{Ca}^{2+}$  release from  $\text{IP}_3$ , but not ryanodine-sensitive intracellular stores in ROS/RNS-induced AIS disruption.

### Calpain, but Not Calcineurin Activity, Is Involved in ROS/RNS-Induced AIS Disruption

While  $\text{Ca}^{2+}$  from both extracellular and intracellular sources appears to play a critical role in ROS/RNS-mediated AIS

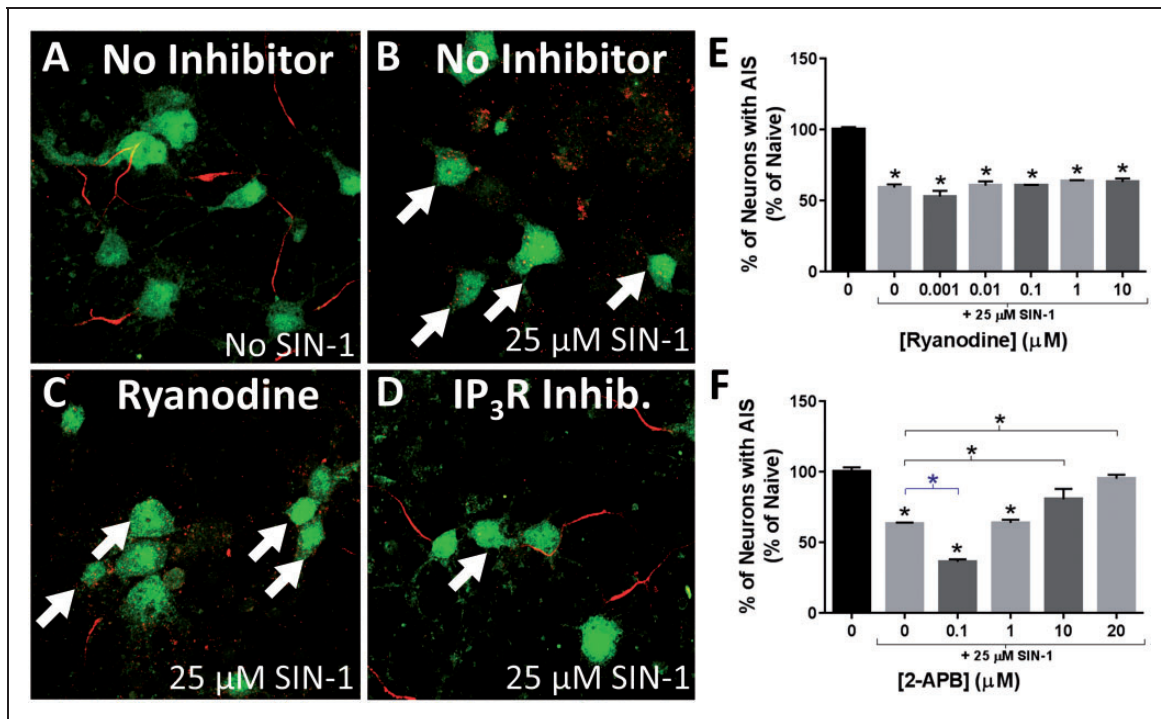


**Figure 5.**  $\text{IP}_3$ -gated  $\text{Ca}^{2+}$  stores are required for ROS/RNS-induced AIS disruption. AIS labeling (AnkG, red) was lost (white arrows) following exposure of cortical neurons (NeuN+, green) to 25  $\mu\text{M}$  SIN-1 (b). This disruption was prevented by pretreatment with an  $\text{IP}_3$ -receptor inhibitor ((d) and (f)) but not an inhibitor to ryanodine receptors ((c) and (e)). Asterisks without an associated bracket represent a significant difference from the SIN-1 untreated group (a,  $*p < .05$ ).

disruption, the downstream mediator of this AIS modulation remains unknown. Previously described mechanisms of AIS plasticity and injury have implicated two  $\text{Ca}^{2+}$ -activated enzymes as critical regulators of AIS stability (Schafer et al., 2009; Evans et al., 2013). These include calcineurin, a  $\text{Ca}^{2+}$ -activated phosphatase responsible for disassembly of the AIS protein complex in models of activity-dependent plasticity (Evans et al., 2013), as well as calpain, a  $\text{Ca}^{2+}$ -activated protease whose substrates include critical structural and functional AIS proteins (Schafer et al., 2009). To assess the contribution of each potential AIS modulator in ROS/RNS-induced AIS disruption, pharmacological inhibitors of each were employed prior to SIN-1 addition. Inhibition of calcineurin with FK-506 (Evans et al., 2013) in the presence of SIN-1 was insufficient to prevent AIS disruption at all concentrations tested (0.001 to 10  $\mu\text{M}$ ; Figure 6(c) and (e)). Concentrations greater than 10  $\mu\text{M}$  resulted in significant neuronal death (data not shown).

Treatment with the well-established calpain inhibitor MDL 28170 (Schafer et al., 2009; Donkor, 2015), however, prevented AIS loss in a dose-dependent manner, at concentrations of 1  $\mu\text{M}$  and 10  $\mu\text{M}$ , yielding preservation of  $83.3\% \pm 0.6\%$  ( $p < .0001$ ) and  $96.8\% \pm 0.8\%$  ( $p < .0001$ ) of AISs, respectively (Figure 6(d) and (f)). A fluorescent activity assay was used to determine the time course of calpain activity, at the time points tested

in Figure 2, in order to correlate with SIN-1-induced AIS loss and recovery. While elevated calpain activity was observed at 12 hr post SIN-1 treatment ( $69.4\% \pm 4.8\%$  increase over untreated;  $p = .0036$ ; Figure 6(g)), peak activity was observed at 24 hr ( $255.5\% \pm 14.9\%$  increase over untreated;  $p < .0001$ ; Figure 6(g)); the time point at which AIS loss is greatest (Figure 2(e) and (j)). Interestingly, by 72 hr post SIN-1 treatment, calpain activity returned to baseline levels ( $34\% \pm 9.9\%$  increase over untreated; Figure 6(g)), corresponding to the point at which neuronal ROS levels returned to baseline (Figure 1(l) and (n)) and AIS recovery is achieved (Figure 2(f) and (k)). Overall, these data implicate a role for calpain, but not calcineurin, as an effector of AIS disruption downstream of oxidative stress.

## Discussion

Previous work from our lab implicated oxidative stress as a mediator of AIS disruption, since free radical scavenger treatment was sufficient to protect and recover the domain in an inflammatory mouse model of MS (Clark et al., 2016). In addition, ablation of NOX2, a major source of ROS/RNS production in the CNS, was sufficient to preserve AIS integrity in an LPS model of systemic inflammation (Benusa et al., 2017). While these studies suggested a

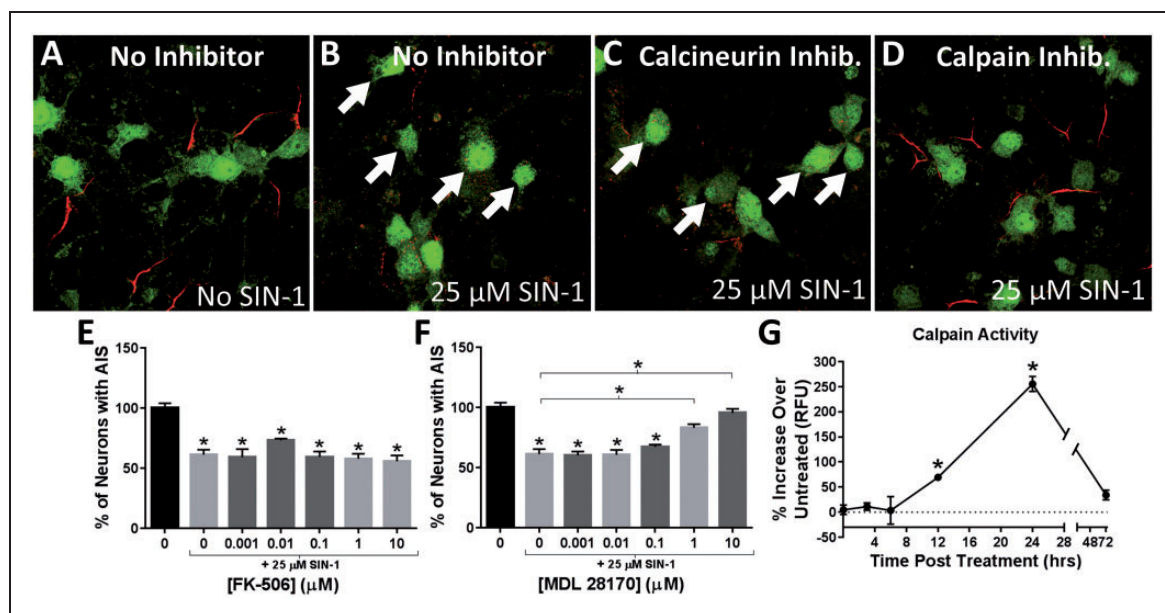


**Figure 6.** ROS/RNS-induced AIS disruption is mediated by calpain but not calcineurin activity. Cultured cortical neurons (NeuN+, green) treated with an inhibitor directed against calcineurin ((c) and (e)) prior to SIN-1 exposure presented with a significant loss (white arrows) of AIS labeling (AnkG, red) similar to the SIN-1 treated neurons without inhibitor pretreatment (b). In contrast, neurons treated with a calpain inhibitor displayed a significant preservation of AISs ((d) and (f)). A calpain protease activity assay revealed significantly elevated activity at 12 hr, peak activity at 24 hr, and a return to baseline by 72 hr post SIN-1 treatment (25  $\mu\text{M}$ ) which is represented as the percent increase over untreated neurons (g). Asterisks without an associated bracket represent a significant difference from the SIN-1 untreated group (a, \* $p < .05$ ).

role for oxidative stress in AIS modulation, the direct effects of reactive oxygen and nitrogen species on AIS stability remained unclear. The present study demonstrates for the first time that oxidative stress, induced through exogenous ROS/RNS application, drives structural alterations of the AIS. In addition, pharmacological inhibition of both voltage-dependent and intracellular  $\text{Ca}^{2+}$  channels suggests that  $\text{Ca}^{2+}$  entry through L-type VDCCs and its release from  $\text{IP}_3$ -gated stores are involved in ROS/RNS-mediated AIS modulation. Furthermore, this AIS insult is dependent upon calpain, but not calcineurin, activity.

### *The Role of ROS/RNS in Axonal Pathology*

The data presented in this study highlight a role for ROS/RNS in disruption of the AIS protein complex, but other axonal targets of oxidative stress have been described. These include the F-actin cytoskeleton (Hung et al., 2011; Sakai et al., 2012), axonal growth cones (Munnamalai and Suter, 2009; Munnamalai et al., 2014), and microtubule-associated stabilizers and motors (Stroissnigg et al., 2007; Carletti et al., 2011; Redondo et al., 2015). Reactive oxygen and nitrogen species have also been associated with the pathogenesis of many CNS insults including axonal loss in peripheral nerve and spinal cord injury (Kuo et al., 2017; Maggio et al., 2017), hyperphosphorylation of tau in Alzheimer's disease (Sepulveda-Diaz et al., 2015), loss of cortical connections following ischemia (Rosenzweig and Carmichael, 2013), and demyelination and axonal degeneration in MS (Forte et al., 2007; Qi et al., 2007).

Because oxidative stress is a key contributor to many CNS pathologies (Lewen et al., 2000; Smith et al., 2013; Mendez-Armenta et al., 2014; Islam, 2017), it is likely that this mechanism of ROS/RNS-induced AIS modulation may underlie many models of CNS injury. Our laboratory has recently identified AIS disruption in both an inflammatory model of MS (Clark et al., 2016), as well as a model of systemic inflammation (Benusa et al., 2017), which was prevented or reversed upon free-radical scavenger treatment. In addition, other labs have reported alterations in AIS stability in models of epilepsy (Wimmer et al., 2010; Harty et al., 2013), ischemic injury (Schafer et al., 2009; Hinman et al., 2013), traumatic brain injury (Baalman et al., 2013; Greer et al., 2013; Vascak et al., 2017), and Alzheimer's disease (Leon-Espinosa et al., 2012; Sun et al., 2014; Marin et al., 2016; Zempel et al., 2017), which have all been shown to be associated with CNS oxidative stress through ROS/RNS dysregulation (Lewen et al., 2000; Smith et al., 2013; Mendez-Armenta et al., 2014; Islam, 2017).

### *ROS/RNS and $\text{Ca}^{2+}$ Entry*

Our data suggest that ROS/RNS-mediated AIS disruption involves extracellular  $\text{Ca}^{2+}$  entry through L-type

VDCCs, as well as intracellular release from  $\text{IP}_3$ -gated stores. While the mechanistic link between ROS/RNS application and cytosolic  $\text{Ca}^{2+}$  levels is not well defined in our system, previous studies examining this link may provide insight. Similar to the present study, SIN-1 treatment is known to induce  $\text{Ca}^{2+}$  entry through L-type channels in CA1 pyramidal neurons, cardiomyocytes, and striatal neurons (Pan et al., 2004; Rocchitta et al., 2005; Zhaowei et al., 2014). Peroxynitrite treatment of cerebral cortical neurons, the cell type used in the present study, also resulted in increased  $\text{Ca}^{2+}$  entry through L-type VDCCs (Ohkuma et al., 2001). However, the effects of SIN-1 have been shown to vary in other cell types, as treatment resulted in decreased  $\text{Ca}^{2+}$  flow through L-type VDCCs in cerebellar granule cells and vestibular hair cells (Gutierrez-Martín et al., 2005; Almanza et al., 2007; Tiago et al., 2011). While the mechanism of ROS/RNS modulation of L-type VDCCs remains unclear for most cell types described, S-glutathionylation of the L-type VDCCs has been shown to be involved in increased  $\text{Ca}^{2+}$  flow through these channels in cardiomyocytes (Tang et al., 2011; Johnstone and Hool, 2014). It remains to be determined if this, or other modifications, could underlie SIN-1-induced  $\text{Ca}^{2+}$  influx through L-type VDCCs in our primary cortical neuron system.

In addition to L-type VDCCs, we demonstrate the involvement of  $\text{IP}_3$ -gated intracellular  $\text{Ca}^{2+}$  stores on ROS/RNS-induced AIS disruption. Similar to the present study, previous work has shown SIN-1 and its ROS/RNS products to induce release of  $\text{Ca}^{2+}$  specifically through  $\text{IP}_3$ -gated stores in neuroblastoma SH-SY5Y cells and cardiomyocytes (Saeki et al., 2000; De Simoni et al., 2013). It has been reported, however, that SIN-1-derived ROS/RNS can induce intracellular  $\text{Ca}^{2+}$  release nonspecifically in renal epithelial cells and ventral horn spinal cord neurons (Ohashi et al., 2016; Munoz et al., 2017) or specifically through ryanodine-sensitive stores in smooth and skeletal muscle cells (Pan et al., 2004; Yamada et al., 2015). Given the cell-type specific effects of ROS/RNS on both voltage-dependent and intracellular  $\text{Ca}^{2+}$  channel function reported in the literature, the mechanistic action of SIN-1 on L-type VDCCs and  $\text{IP}_3$ -gated intracellular stores in our system remains to be determined.

### *How Does Calpain Modulate the AIS?*

In the present study, we have identified ROS/RNS-induced AIS disruption to be dependent upon calpain activation. Similarly, calpain activity has been shown to drive AIS alterations in other model systems including ischemic injury (Schafer et al., 2009), glutamate excitotoxicity (Bened-Jensen et al., 2016), and P2X7 purinergic activation (Del Puerto et al., 2015). Schafer et al. (2009) demonstrated that proteolytic degradation of

essential AIS proteins, such as ankyrinG,  $\beta$ IV spectrin, and voltage-gated  $\text{Na}^+$  channels, was the mechanism underlying calpain-mediated AIS modulation following ischemic injury. Benned-Jensen et al. (2016) and Del Puerto et al. (2015) did not analyze the extent of proteolysis, but speculated that a mechanism similar to that reported by Schafer et al. (2009) was most likely involved in their models of AIS injury. It is likely that calpain-mediated proteolysis of the AIS complex underlies the alterations observed following the ROS/RNS-induced insult presented in this study, as this mechanism is well characterized by Schafer et al. (2009).

In summary, for the first time, we demonstrate that oxidative stress, stimulated directly through exogenously applied ROS/RNS, is capable of reversible structural modulation of the AIS. This mechanism involves activity of L-type VDCCs, as well as intracellular  $\text{IP}_3$ -gated stores. In addition, calpain, but not calcineurin, activity is involved in this ROS/RNS-induced disruption. These findings provide new insights into the mechanisms underlying altered AIS stability in a variety of CNS pathologies.

## Summary

Oxidative stress, stimulated through the exogenous application of reactive oxygen and nitrogen species, drives structural disruption of the axon initial segment through a  $\text{Ca}^{2+}$  and calpain-dependent mechanism.

## Acknowledgments

The authors wish to thank Dr. Matthew Rasband, Professor in the Department of Neuroscience, Baylor College of Medicine, for his generous gift of the  $\beta$ IV spectrin antibody.

## Declaration of Conflicting Interests

The author(s) declared no potential conflicts of interest with respect to the research, authorship, and/or publication of this article.

## Funding

The author(s) disclosed receipt of the following financial support for the research, authorship, and/or publication of this article: This study was supported by a Veterans Affairs Merit Award (51O1BX002565). Microscopy was performed at the Virginia Commonwealth University –Department of Anatomy and Neurobiology Microscopy Facility, supported, in part, with funding from NIH-NINDS Center core grant (5P30NS047463).

## Supplemental Material

Supplementary material is available for this article online.

## References

- Almanza, A., Navarrete, F., Vega, R., & Soto, E. (2007). Modulation of voltage-gated  $\text{Ca}^{2+}$  current in vestibular hair cells by nitric oxide. *J Neurophysiol*, *97*, 1188–1195.

- Baalman, K. L., Cotton, R. J., Rasband, S. N., & Rasband, M. N. (2013). Blast wave exposure impairs memory and decreases axon initial segment length. *J Neurotrauma*, *30*, 741–751.
- Benned-Jensen, T., Christensen, R. K., Denti, F., Perrier, J. F., Rasmussen, H. B., & Olesen, S. P. (2016). Live imaging of Kv7.2/7.3 cell surface dynamics at the axon initial segment: High steady-state stability and calpain-dependent excitotoxic downregulation revealed. *J Neurosci*, *36*, 2261–2266.
- Benusa, S. D., George, N. M., Sword, B. A., DeVries, G. H., & Dupree, J. L. (2017). Acute neuroinflammation induces AIS structural plasticity in a NOX2-dependent manner. *J Neuroinflammation*, *14*, 116.
- Bhattacharjee, A., Whitehurst, R. M. Jr., Zhang, M., Wang, L., & Li, M. (1997). T-type calcium channels facilitate insulin secretion by enhancing general excitability in the insulin-secreting beta-cell line, INS-1. *Endocrinology*, *138*, 3735–3740.
- Buffington, S. A., & Rasband, M. N. (2011). The axon initial segment in nervous system disease and injury. *Eur J Neurosci*, *34*, 1609–1619.
- Carletti, B., Passarelli, C., Sparaco, M., Tozzi, G., Pastore, A., Bertini, E., & Piemonte, F. (2011). Effect of protein glutathionylation on neuronal cytoskeleton: A potential link to neurodegeneration. *Neuroscience*, *192*, 285–294.
- Catterall, W. A. (2011). Voltage-gated calcium channels. *Cold Spring Harb Perspect Biol*, *3*, a003947.
- Clark, K. C., Josephson, A., Benusa, S. D., Hartley, R. K., Baer, M., Thummala, S., Joslyn, M., Sword, B. A., Elford, H., Oh, U., Dilsizoglu-Senol, A., Lubetzki, C., Davenne, M., DeVries, G. H., & Dupree, J. L. (2016). Compromised axon initial segment integrity in EAE is preceded by microglial reactivity and contact. *Glia*, *64*, 1190–1209.
- De Simoni, S., Linard, D., Hermans, E., Knoops, B., & Goemaere, J. (2013). Mitochondrial peroxiredoxin-5 as potential modulator of mitochondria-ER crosstalk in MPP<sup>+</sup>-induced cell death. *J Neurochem*, *125*, 473–485.
- DeHaven, W. I., Smyth, J. T., Boyles, R. R., Bird, G. S., & Putney, J. W. Jr. (2008). Complex actions of 2-aminoethylidiphenyl borate on store-operated calcium entry. *J Biol Chem*, *283*, 19265–19273.
- Del Puerto, A., Fronzaroli-Molinieres, L., Perez-Alvarez, M. J., Giraud, P., Carlier, E., Wandosell, F., Debanne, D., & Garrido, J. J. (2015). ATP-P2X7 receptor modulates axon initial segment composition and function in physiological conditions and brain injury. *Cereb Cortex*, *25*, 2282–2294.
- Donkor, I. O. (2015). An updated patent review of calpain inhibitors (2012–2014). *Expert Opin Ther Pat*, *25*, 17–31.
- Evans, M. D., Sammons, R. P., Lebron, S., Dumitrescu, A. S., Watkins, T. B., Uebele, V. N., Renger, J. J., & Grubb, M. S. (2013). Calcineurin signaling mediates activity-dependent relocation of the axon initial segment. *J Neurosci*, *33*, 6950–6963.
- Forte, M., Gold, B. G., Marracci, G., Chaudhary, P., Basso, E., Johnsen, D., Yu, X., Fowlkes, J., Rahder, M., Stem, K., Bernardi, P., & Bourdette, D. (2007). Cyclophilin D inactivation protects axons in experimental autoimmune encephalomyelitis, an animal model of multiple sclerosis. *Proc Natl Acad Sci U S A*, *104*, 7558–7563.
- Fusi, F., Trezza, A., Spiga, O., Sgaragli, G., & Bova, S. (2017). Cav1.2 channel current block by the PKA inhibitor H-89 in rat tail artery myocytes via a PKA-independent mechanism:

- Electrophysiological, functional, and molecular docking studies. *Biochem Pharmacol*, 140, 53–63.
- Greer, J. E., Hanell, A., McGinn, M. J., & Povlishock, J. T. (2013). Mild traumatic brain injury in the mouse induces axotomy primarily within the axon initial segment. *Acta Neuropathol*, 126, 59–74.
- Gutierrez-Martin, Y., Martin-Romero, F. J., Henao, F., & Gutierrez-Merino, C. (2005). Alteration of cytosolic free calcium homeostasis by SIN-1: High sensitivity of L-type  $\text{Ca}^{2+}$  channels to extracellular oxidative/nitrosative stress in cerebellar granule cells. *J Neurochem*, 92, 973–989.
- Hamada, M. S., & Kole, M. H. (2015). Myelin loss and axonal ion channel adaptations associated with gray matter neuronal hyperexcitability. *J Neurosci*, 35, 7272–7286.
- Harty, R. C., Kim, T. H., Thomas, E. A., Cardamone, L., Jones, N. C., Petrou, S., & Wimmer, V. C. (2013). Axon initial segment structural plasticity in animal models of genetic and acquired epilepsy. *Epilepsy Res*, 105, 272–279.
- Hedstrom, K. L., Ogawa, Y., & Rasband, M. N. (2008). AnkyrinG is required for maintenance of the axon initial segment and neuronal polarity. *J Cell Biol*, 183, 635–640.
- Hinman, J. D., Rasband, M. N., & Carmichael, S. T. (2013). Remodeling of the axon initial segment after focal cortical and white matter stroke. *Stroke*, 44, 182–189.
- Hung, R. J., Pak, C. W., & Terman, J. R. (2011). Direct redox regulation of F-actin assembly and disassembly by mical. *Science*, 334, 1710–1713.
- Isaev, N. K., Genrikhs, E. E., Aleksandrova, O. P., Zelenova, E. A., & Stelmashook, E. V. (2016). Glucose deprivation stimulates  $\text{Cu}^{2+}$  toxicity in cultured cerebellar granule neurons and  $\text{Cu}^{2+}$ -dependent zinc release. *Toxicol Lett*, 250–251, 29–34.
- Islam, M. T. (2017). Oxidative stress and mitochondrial dysfunction-linked neurodegenerative disorders. *Neurol Res*, 39, 73–82.
- Jenkins, S. M., & Bennett, V. (2001). Ankyrin-G coordinates assembly of the spectrin-based membrane skeleton, voltage-gated sodium channels, and L1 CAMs at purkinje neuron initial segments. *J Cell Biol*, 155, 739–746.
- Johnstone, V. P., & Hool, L. C. (2014). Glutathionylation of the L-type  $\text{Ca}^{2+}$  channel in oxidative stress-induced pathology of the heart. *Int J Mol Sci*, 15, 19203–19225.
- Kipp, M., Nyamoya, S., Hochstrasser, T., & Amor, S. (2017). Multiple sclerosis animal models: A clinical and histopathological perspective. *Brain Pathol*, 27, 123–137.
- Kuo, C. C., Su, H. L., Chang, T. L., Chiang, C. Y., Sheu, M. L., Cheng, F. C., Chen, C. J., Sheehan, J., & Pan, H. C. (2017). Prevention of axonal degeneration by perineurium injection of mitochondria in a sciatic nerve crush injury model. *Neurosurgery*, 80, 475–488.
- Leon-Espinosa, G., DeFelipe, J., & Munoz, A. (2012). Effects of amyloid-beta plaque proximity on the axon initial segment of pyramidal cells. *J Alzheimers Dis*, 29, 841–852.
- Lewen, A., Matz, P., & Chan, P. H. (2000). Free radical pathways in CNS injury. *J Neurotrauma*, 17, 871–890.
- Liu, Y., Lu, L., Hettinger, C. L., Dong, G., Zhang, D., Rezvani, K., Wang, X., & Wang, H. (2014). Ubiquilin-1 protects cells from oxidative stress and ischemic stroke caused tissue injury in mice. *J Neurosci*, 34, 2813–2821.
- Maggio, D. M., Singh, A., Iorgulescu, J. B., Bleicher, D. H., Ghosh, M., Lopez, M. M., Tuesta, L. M., Flora, G., Dietrich, W. D., & Pearce, D. D. (2017). Identifying the long-term role of inducible nitric oxide synthase after contusive spinal cord injury using a transgenic mouse model. *Int J Mol Sci*, 18, 245 doi:10.3390/ijms18020245.
- Marin, M. A., Ziburkus, J., Jankowsky, J., & Rasband, M. N. (2016). Amyloid-beta plaques disrupt axon initial segments. *Exp Neurol*, 281, 93–98.
- Marks, A. R. (1997). Intracellular calcium-release channels: Regulators of cell life and death. *Am J Physiol*, 272, H597–H605.
- Matsebatlela, T. M., Anderson, A. L., Gallicchio, V. S., Elford, H., & Rice, C. D. (2015). 3,4-dihydroxy-benzohydroxamic acid (didox) suppresses pro-inflammatory profiles and oxidative stress in TLR4-activated RAW264.7 murine macrophages. *Chem Biol Interact*, 233, 95–105.
- Mayhew, C. N., Mampuru, L. J., Chendil, D., Ahmed, M. M., Phillips, J. D., Greenberg, R. N., Elford, H. L., & Gallicchio, V. S. (2002). Suppression of retrovirus-induced immunodeficiency disease (murine AIDS) by trimidox and didox: Novel ribonucleotide reductase inhibitors with less bone marrow toxicity than hydroxyurea. *Antiviral Res*, 56, 167–181.
- Mendez-Armenta, M., Nava-Ruiz, C., Juarez-Rebollar, D., Rodriguez-Martinez, E., & Gomez, P. Y. (2014). Oxidative stress associated with neuronal apoptosis in experimental models of epilepsy. *Oxid Med Cell Longev*, 2014, 293689.
- Munnamalai, V., & Suter, D. M. (2009). Reactive oxygen species regulate F-actin dynamics in neuronal growth cones and neurite outgrowth. *J Neurochem*, 108, 644–661.
- Munnamalai, V., Weaver, C. J., Weisheit, C. E., Venkatraman, P., Agim, Z. S., Quinn, M. T., & Suter, D. M. (2014). Bidirectional interactions between NOX2-type NADPH oxidase and the F-actin cytoskeleton in neuronal growth cones. *J Neurochem*, 130, 526–540.
- Munoz, F. M., Zhang, F., Islas-Robles, A., Lau, S. S., & Monks, T. J. (2017). Ros-induced store-operated  $\text{Ca}^{2+}$  entry coupled to parp-1 hyperactivation is independent of parg activity in necrotic cell death. *Toxicol Sci*, 158, 444–453.
- Nguemo, F., Fleischmann, B. K., Gupta, M. K., Saric, T., Malan, D., Liang, H., Pfannkuche, K., Bloch, W., Schunkert, H., Hescheler, J., & Reppel, M. (2013). The L-type  $\text{Ca}^{2+}$  channels blocker nifedipine represses mesodermal fate determination in murine embryonic stem cells. *PLoS One*, 8, e53407.
- Ohashi, M., Hirano, T., Watanabe, K., Katsumi, K., Ohashi, N., Baba, H., Endo, N., & Kohno, T. (2016). Hydrogen peroxide modulates synaptic transmission in ventral horn neurons of the rat spinal cord. *J Physiol*, 594, 115–134.
- Ohkuma, S., Katsura, M., Higo, A., Shirotani, K., Hara, A., Tarumi, C., & Ohgi, T. (2001). Peroxynitrite affects  $\text{Ca}^{2+}$  influx through voltage-dependent calcium channels. *J Neurochem*, 76, 341–350.
- Pan, B. X., Zhao, G. L., Huang, X. L., & Zhao, K. S. (2004). Calcium mobilization is required for peroxynitrite-mediated enhancement of spontaneous transient outward currents in arteriolar smooth muscle cells. *Free Radic Biol Med*, 37, 823–838.
- Pollock, J. D., Williams, D. A., Gifford, M. A., Li, L. L., Du, X., Fisherman, J., Orkin, S. H., Doerschuk, C. M., & Dinauer, M. C. (1995). Mouse model of X-linked chronic granulomatous disease, an inherited defect in phagocyte superoxide production. *Nat Genet*, 9, 202–209.

- Qi, X., Lewin, A. S., Sun, L., Hauswirth, W. W., & Guy, J. (2007). Suppression of mitochondrial oxidative stress provides long-term neuroprotection in experimental optic neuritis. *Invest Ophthalmol Vis Sci*, *48*, 681–691.
- Ravens, U., & Schopper, H. P. (1990). Opposite cardiac actions of the enantiomers of bay K 8644 at different membrane potentials in guinea-pig papillary muscles. *Naunyn Schmiedebergs Arch Pharmacol*, *341*, 232–239.
- Redondo, J., Hares, K., Wilkins, A., Scolding, N., & Kemp, K. (2015). Reductions in kinesin expression are associated with nitric oxide-induced axonal damage. *J Neurosci Res*, *93*, 882–892.
- Rocchitta, G., Migheli, R., Mura, M. P., Grella, G., Esposito, G., Marchetti, B., Miele, E., Desole, M. S., Miele, M., & Serra, P. A. (2005). Signaling pathways in the nitric oxide and iron-induced dopamine release in the striatum of freely moving rats: Role of extracellular  $\text{Ca}^{2+}$  and L-type  $\text{Ca}^{2+}$  channels. *Brain Res*, *1047*, 18–29.
- Rosenzweig, S., & Carmichael, S. T. (2013). Age-dependent exacerbation of white matter stroke outcomes: A role for oxidative damage and inflammatory mediators. *Stroke*, *44*, 2579–2586.
- Saeki, M., Kamisaki, Y., & Maeda, S. (2000). Potentiation of carbachol-induced  $\text{Ca}^{2+}$  release by peroxynitrite in human neuroblastoma SH-SY5Y cells. *Neurochem Res*, *25*, 909–914.
- Sakai J., Li J., Subramanian K. K., Mondal S., Bajrami B., Hattori H., Jia Y., Dickinson BC, Zhong J, Ye K, Chang CJ, Ho Y. S., Zhou J., & Luo H. R. (2012) Reactive oxygen species-induced actin glutathionylation controls actin dynamics in neutrophils. *Immunity*, *37*, 1037–1049.
- Schafer, D. P., Jha, S., Liu, F., Akella, T., McCullough, L. D., & Rasband, M. N. (2009). Disruption of the axon initial segment cytoskeleton is a new mechanism for neuronal injury. *J Neurosci*, *29*, 13242–13254.
- Sepulveda-Diaz, J. E., Alavi Naini, S. M., Huynh, M. B., Ouidja, M. O., Yanicostas, C., Chantepie, S., Villares, J., Lamari, F., Jospin, E., van Kuppevelt, T. H., Mensah-Nyagan, A. G., Raisman-Vozari, R., Soussi-Yanicostas, N., & Papy-Garcia, D. (2015). HS3ST2 expression is critical for the abnormal phosphorylation of tau in alzheimer's disease-related tau pathology. *Brain*, *138*, 1339–1354.
- Shepherd, M. N., Pomicter, A. D., Velazco, C. S., Henderson, S. C., & Dupree, J. L. (2012). Paranodal reorganization results in the depletion of transverse bands in the aged central nervous system. *Neurobiol Aging*, *33*, 203.e13–203.e24.
- Singh, R. J., Hogg, N., Joseph, J., Konorev, E., & Kalyanaraman, B. (1999). The peroxynitrite generator, SIN-1, becomes a nitric oxide donor in the presence of electron acceptors. *Arch Biochem Biophys*, *361*, 331–339.
- Smith, J. A., Park, S., Krause, J. S., & Banik, N. L. (2013). Oxidative stress, DNA damage, and the telomeric complex as therapeutic targets in acute neurodegeneration. *Neurochem Int*, *62*, 764–775.
- Stoler, O., & Fleidervish, I. A. (2016). Functional implications of axon initial segment cytoskeletal disruption in stroke. *Acta Pharmacol Sin*, *37*, 75–81.
- Stroissnigg, H., Trancikova, A., Descovich, L., Fuhrmann, J., Kutschera, W., Kostan, J., Meixner, A., Nothias, F., & Propst, F. (2007). S-nitrosylation of microtubule-associated protein 1B mediates nitric-oxide-induced axon retraction. *Nat Cell Biol*, *9*, 1035–1045.
- Sun, X., Wu, Y., Gu, M., Liu, Z., Ma, Y., Li, J., & Zhang, Y. (2014). Selective filtering defect at the axon initial segment in alzheimer's disease mouse models. *Proc Natl Acad Sci U S A*, *111*, 14271–14276.
- Tang, H., Viola, H. M., Filipovska, A., & Hool, L. C. (2011). Ca(v)1.2 calcium channel is glutathionylated during oxidative stress in guinea pig and ischemic human heart. *Free Radic Biol Med*, *51*, 1501–1511.
- Tiago, T., Marques-da-Silva, D., Samhan-Arias, A. K., Aureliano, M., & Gutierrez-Merino, C. (2011). Early disruption of the actin cytoskeleton in cultured cerebellar granule neurons exposed to 3-morpholinopyridone-oxidative stress is linked to alterations of the cytosolic calcium concentration. *Cell Calcium*, *49*, 174–183.
- Trackey, J. L., Uliasz, T. F., & Hewett, S. J. (2001). SIN-1-induced cytotoxicity in mixed cortical cell culture: Peroxynitrite-dependent and -independent induction of excitotoxic cell death. *J Neurochem*, *79*, 445–455.
- Turchan, J., Pocernich, C. B., Gairola, C., Chauhan, A., Schifitto, G., Butterfield, D. A., Buch, S., Narayan, O., Sinai, A., Geiger, J., Berger, J. R., Elford, H., & Nath, A. (2003). Oxidative stress in HIV demented patients and protection ex vivo with novel antioxidants. *Neurology*, *60*, 307–314.
- Vascak, M., Sun, J., Baer, M., Jacobs, K. M., & Povlishock, J. T. (2017). Mild traumatic brain injury evokes pyramidal neuron axon initial segment plasticity and diffuse presynaptic inhibitory terminal loss. *Front Cell Neurosci*, *11*, 157.
- Wimmer, V. C., Reid, C. A., So, E. Y., Berkovic, S. F., & Petrou, S. (2010). Axon initial segment dysfunction in epilepsy. *J Physiol*, *588*, 1829–1840.
- Yamada, R., & Kuba, H. (2016). Structural and functional plasticity at the axon initial segment. *Front Cell Neurosci*, *10*, 250.
- Yamada, T., Fedotovskaya, O., Cheng, A. J., Cornachione, A. S., Minozzo, F. C., Aulin, C., Friden, C., Turesson, C., Andersson, D. C., Glenmark, B., Lundberg, I. E., Rassier, D. E., Westerblad, H., & Lanner, J. T. (2015). Nitrosative modifications of the  $\text{Ca}^{2+}$  release complex and actin underlie arthritis-induced muscle weakness. *Ann Rheum Dis*, *74*, 1907–1914.
- Zempel, H., Dennissen, F., Kumar, Y., Luedtke, J., Biernat, J., Mandelkow, E. M., & Mandelkow, E. (2017). Axodendritic sorting and pathological missorting of tau is isoform specific and determined by axon initial segment architecture. *J Biol Chem*, *292*, 12192–12207.
- Zhaowei, L., Yongling, X., Jiajia, Y., & Zhuo, Y. (2014). The reduction of EPSC amplitude in CA1 pyramidal neurons by the peroxynitrite donor SIN-1 requires  $\text{Ca}^{2+}$  influx via postsynaptic non-L-type voltage gated calcium channels. *Neurochem Res*, *39*, 361–371.